Application of a Large Eddy Simulation Model to Study Room Airflow

Steven J. Emmerich
Associate Member ASHRAE

Kevin B. McGrattan

ABSTRACT

A three-dimensional, large eddy simulation (LES) model developed for studying the transport of smoke and hot gases during a fire in an enclosure is described. The model uses finite difference techniques to solve the Navier-Stokes equations with an approach emphasizing high spatial resolution and efficient flow-solving techniques. The model uses the Smagorinsky subgrid-scale model.

The LES model with Smagorinsky subgrid-scale model was applied to ventilation airflow in a three-dimensional room. Airflow results were in excellent agreement with both measured values and LES simulations with the more complicated, dynamic SGS model (reported by Davidson and Nielsen 1996) in the main portion of the room. Agreement was not as good near the floor and ceiling; however, no empirical near-wall model was used. Also, some interaction between Smagorinsky constant and grid resolution was found.

INTRODUCTION

There are two general types of computer simulation techniques for studying airflow and contaminant transport in buildings—multizone modeling and room airflow modeling. Multizone modeling takes a macroscopic view of indoor air quality (IAQ) by evaluating average pollutant concentrations in the different zones of a building as contaminants are transported through the building and its HVAC system. Room airflow modeling takes a microscopic view of IAQ by applying a computational fluid dynamics (CFD) program to examine the detailed flow fields and pollutant concentration distributions within a room or rooms. Each approach has strengths and limitations for studying different building ventilation and IAQ problems.

The National Institute of Standards and Technology (NIST) has maintained a strong multizone modeling effort with the continuing development and application of the CONTAM program (Walton 1994). Several years ago, a CFD program called EXACT3 was developed for studying room airflows and was applied to the prediction of ventilation system performance in an open office space (Kurabuchi et al. 1990). EXACT3 employed a k-ε turbulence model that, at the time, was considered the only practical method for modeling turbulent airflows. Recently, a CFD program has been developed at NIST to simulate the transport of smoke and hot gases during a fire in an enclosure (McGrattan et al. 1994). This new CFD model employs highly efficient solution procedures and a technique, called large eddy simulation (LES), to more accurately simulate the temporal and spatial variations of the flow field. A project was undertaken at NIST to investigate options for using this program (referred to in this paper as NIST-LES3D) for studying building ventilation and indoor air quality.

This paper contains a brief discussion of CFD theory, summarizes relevant findings of a literature review performed to learn the current state of CFD research in the building ventilation and IAQ fields, describes the NIST-LES3D program, and presents the application of NIST-LES3D to a three-dimensional ventilated room.

CFD THEORY

This section contains a brief introduction to computational fluid dynamics (CFD) theory. A thorough treatment may be found in many textbooks on the subject, such as Anderson et al. (1984) or in an earlier NIST report (Kurabuchi et al. 1990). CFD is the application of numerical techniques to solve the Navier-Stokes equations for fluid flow. The Navier-Stokes equations are derived by applying the principles of

Steven J. Emmerich and **Kevin B. McGrattan** are research engineers in the Building and Fire Research Laboratory, National Institute of Standards and Technology, Gaithersburg, Md.

conservation of mass and momentum to a control volume of fluid. When applying CFD to the IAQ field, conservation of mass for a contaminant species and energy for thermal responses also may be applied, but they will not be included here.

In CFD, the Navier-Stokes equations are solved by discretizing the equations using either finite difference or finite element techniques. Direct numerical simulation (DNS) involves solving these equations directly with the problem discretized to a grid fine enough to capture the smallest possible turbulent eddy. The eddy size may be estimated from dimensional analysis to be on the order of the Kolmogorov length scale $((\nu^3/\varepsilon)^{1/4}$ where ν is viscosity and ε is the dissipation rate of turbulence energy and is typically 10^{-2} m to 10^{-3} m (Tennekes and Lumley 1972).

Performing a DNS for the airflow in a room is a formidable task even for modern computing power. Therefore, various other approaches have been used to model turbulence. The most widely applied turbulence modeling technique is the k-ε model (where k is the turbulent kinetic energy and ε is the dissipation rate of turbulent energy). This model usually is available in all commercial CFD programs and in most research codes, although other turbulence models also may be offered. As with the general theory of CFD, the details of the k-ε model are presented elsewhere (e.g., Kurabuchi et al. 1990) and only a general description will be included here.

The k-ε model is derived by substituting the sum of an average term plus a fluctuating term for the instantaneous quantities in Equations 1 and 2 shown in "Mathematical Model" below (e.g., $U_i = u_i + u'_i$). The average terms are expected to vary less than the instantaneous quantities and, therefore, can be resolved over a coarser grid. However, this averaging procedure yields an additional unknown term called the Reynolds stress ($-\rho u'_i u'_i$). The additional unknowns are resolved by introducing the eddy viscosity concept, which results in two additional transport equations, one each for k and ε, and five empirical constants.

Although the k-ε model is an empirical formulation, it has been used successfully to model turbulent flow in many different situations including room airflow. However, there also have been problems applying the k-ε model to room airflow simulation, as highlighted by Moser (1991) in a summary of International Energy Agency (IEA) Annex 20, "Airflow Patterns within Buildings." Moser concluded that the accurate simulation of room airflow with forced convection with a k-ε turbulence model was possible, but problems included turbulence modeling at low Reynolds numbers and in the near-wall region and modeling natural and mixed convection. In response to these problems, researchers have extended the k-ε model specifically for situations of low Reynolds numbers, near-wall regions, and natural convection. While they have had some success, the result is a more empirical and less general model.

An alternative to DNS and the k-ε turbulence model is large eddy simulation (Smagorinsky et al. 1965; Deardorff 1970). The LES method involves solution of the time-dependent Navier-Stokes equations spatially filtered over the computational grid. The effect of subgrid-scale (SGS) motion is approximated though a SGS eddy viscosity model.

Kurabuchi and Kusuda (1987) cite the advantages of the LES model as being direct use of the filtered Navier-Stokes equations, only one empirical constant, and more universal and acceptable modeling for the SGS stresses than those required in other turbulence models. The primary disadvantage they mention is the greater computational difficulty, which they see limiting the method to problems requiring very fundamental understanding of flow phenomena or verification of simpler models. An important fundamental difference between the LES and typical k-ε methods is the treatment of the time-dependency of the problem. The typical k-ε method results in a "steady-state" solution to an averaged version of the flow equations, while the LES results in a transient solution to the actual Navier-Stokes equations. Because real turbulent flow situations are inherently transient, LES methods could have an advantage in modeling turbulent flow.

Literature Review

An extensive literature review on the application of CFD to building ventilation and IAQ problems was performed recently (Emmerich 1997). Applications discussed in the literature include room airflow case studies involving calculation of airflow patterns, temperatures, ventilation system performance and thermal comfort for various ventilation systems, and strategies and room configurations; flow from diffusers; modeling effects of occupants; exhaust ventilation system performance; wind pressure distribution for flow around buildings; thermal and airflow performance in large enclosures; pollutant transport including particles and moisture; air curtains; pressure loss in ducts; and coupling of CFD programs with multizone airflow models and/or building energy simulation models. A number of applications of advanced turbulence models to room airflow problems are summarized below. One significant development in the literature is recent studies that found LES results agree better with experimental results for situations examined. These reports indicate that the research community is moving toward the application of LES methods.

Turbulence Modeling

In a summary of IEA Annex 20 research, Moser (1991) identified turbulence modeling as one of five major technical problems encountered (only the k-ε turbulence model was used). Problems with the standard k-ε turbulence model have been identified by others and have led to research on modified versions and advanced turbulence models. Studies considering the LES model are discussed in a separate section below.

Murakami et al. (1994) compared the capability of three turbulence models, including the k-ε eddy viscosity model (EVM), the algebraic stress model (ASM), and the differential stress model (DSM), at predicting the flow in a room with a

horizontal, nonisothermal jet from a diffuser. The ASM adds consideration of anisotropy of Reynolds stresses to the k-ε model through additional algebraic equations. The DSM, also called the Reynolds stress model (RSM), uses time-averaged Navier-Stokes equations with differential equations to consider anisotropy of Reynolds stresses. Measurements and predictions indicated that the DSM model predicted the velocity distribution best, both DSM and ASM predicted temperatures better than k-ε, and the k-ε could not predict the anisotropic nature of the Reynolds stress in the jet.

Xu et al. (1994) simulated isothermal airflow in a room using the standard k-ε model and three different low Reynolds number k-ε models. All four models were in good agreement for predictions of the velocity field. The low Reynolds number models overpredicted the turbulence kinetic energy in the boundary layers.

Stathopoulos and Zhou (1995) and Zhou and Stathopoulos (1996) compared predictions of the wind-induced pressure on the roof of a building for various versions of the k-ε turbulence model to measurements. They reported poor performance with the standard model but better predictions with a "two-layer" method combining the k-ε model with either a one-equation model or a low Reynolds number model in the near-wall area.

Buchmann et al. (1994) found that a low Reynolds number turbulence model improved predictions compared to the standard k-ε model for a large enclosure. In a comparison of several turbulence models, Chen and Chao (1996) found that a Reynolds stress model performed best for a turbulent buoyant plume case, while a renormalization group (RNG) k-ε model performed best for a displacement ventilation room case.

Takemasa et al. (1992) evaluated the accuracy of different wall functions in conjunction with the k-ε turbulence model at predicting convective wall heat flows in both heated and cooled rooms. They concluded that a wall function that depends on turbulence energy at wall-adjacent nodes and takes into account viscous sublayer thickness produces the most satisfactory results.

Large Eddy Simulation

Recently, a few studies have applied CFD models with LES turbulence modeling to building ventilation and IAQ research topics. In an early report, Sakamoto and Matsuo (1980) compared predictions of isothermal flow in a simple ventilated room using both the k-ε turbulence model and a large eddy simulation model to measurements. They concluded that both methods showed "good" agreement with the experimental results without a noticeable difference between the two methods with regard to mean velocity. However, both methods had difficulty near the exhaust inlet, and the LES model corresponded better with the experimental results around the supply outlet.

Davidson and Nielsen (1996) report a recent simulation effort employing LES modeling of airflow in a three-dimensional ventilated room. Simulations of a test case were performed at two levels of grid refinement and with two LES subgrid-scale models (Smagorinsky and dynamic). The dynamic SGS model depends on a parameter that is computed from the actual flow conditions rather than chosen as a constant in advance. This parameter can vary in both time and space but requires more computation time. Some flow results are presented for a simple test case and compared to measurement. The authors concluded that the Smagorinsky subgrid model was inadequate, but the results obtained with the dynamic subgrid model were in good agreement with measurements.

Bennetsen et al. (1996) also studied the application of LES to a three-dimensional room airflow test case. Simulations were performed with Smagorinsky, mixed-scale, and dynamic subgrid models and the results were compared to CFD simulations employing the standard k-ε model, the low-Reynolds number k-ε model, a renormalization group k-ε model, and experimental measurements. The authors found that the LES with a dynamic model agreed "quite well" with measurements, but the LES with Smagorinsky and mixed-scale models suffered from inadequate grid resolution.

Murakami et al. (1996) compare predictions for flow around a building using CFD with four turbulence models (k-ε EVM, ASM, DSM, and LES) to measurements from wind tunnel tests. Comparisons are presented for mean velocity vectors, turbulent kinetic energy, mean surface pressure distribution, turbulence energy production, and normal stress components. They concluded that the LES agrees well with experimental measurements, the k-ε EVM included several serious discrepancies due to the isotropic eddy viscosity hypothesis, some inaccuracies still exist in results of ASM, and DSM improved on some aspects of ASM but was worse on others.

NIST-LES3D PROGRAM DESCRIPTION

Recently, researchers at NIST have developed a CFD code using the LES method to simulate the transport of smoke and hot gases during a fire in an enclosure (McGrattan et al. 1994). The approach emphasizes the use of high spatial and temporal resolution and efficient flow-solving techniques while limiting the use of empirical models. The key to the approach is limiting the problem to regular rectangular, cylindrical, or spherical geometry. The grid must be uniform in the horizontal direction but may be varied in the vertical direction. This restriction is necessary in order to use a Fast Fourier Transform (FFT)-based Poisson solver for the pressure instead of an iterative solution. The fast solution enables use of high grid resolution fine enough to capture all "important eddies." It is not possible to capture all eddies, but extremely small ones have little influence on bulk properties of most problems (temperature and contaminant distribution). Currently, the SGS model options include a constant eddy viscosity model and the Smagorinsky model.

Mathematical Model

Consider a thermally expandable ideal gas driven by a prescribed heat source. The equations of motion governing the fluid flow are written in a form suitable for low Mach number applications (Rehm and Baum 1978). Sometimes this form of the equations is referred to as "weakly compressible." The most important feature of these equations is that in the energy and state equations, the spatially and temporally varying pressure is replaced by an average pressure that depends only on time. This is done to filter out acoustic waves. The efficiency of the numerical solution of the equations is increased dramatically by this approximation.

In the equations to follow, all symbols have their usual fluid dynamic meaning: ρ is the density, $\boldsymbol{u}$ the velocity vector, $\boldsymbol{\varpi}$ the vorticity, p the pressure, $\boldsymbol{g}$ the gravity vector, c_p the constant-pressure specific heat, T the temperature, k the thermal conductivity, t the time, $\dot{q}$ the prescribed volumetric heat release, R the gas constant equal to the difference of the specific heats (c_p - c_v), and σ the standard stress tensor for compressible fluids. The model starts with the application of the conservation of mass, momentum, and energy to a control volume of fluid (Equations 1 through 3) and the equation of state (Equation 4).

$$\frac{\partial \rho}{\partial t} + \nabla \cdot \rho \boldsymbol{u} = 0 \tag{1}$$

$$\rho\left(\frac{\partial \boldsymbol{u}}{\partial t} + \frac{1}{2}\nabla|\boldsymbol{u}|^2 - \boldsymbol{u} \times \omega\right) + \nabla p - \rho \boldsymbol{g} = \nabla \cdot \boldsymbol{\sigma} \tag{2}$$

$$\rho c_p\left(\frac{\partial T}{\partial t} + \boldsymbol{u} \cdot \nabla T\right) - \frac{dp_o}{dt} = \dot{q} + \nabla \cdot k \nabla T \tag{3}$$

$$p_o(t) = \rho R T \tag{4}$$

The divergence of the flow is a very important quantity in the analysis to follow, and it is found by taking the total derivative of Equation 4 and substituting expressions from Equations 1 and 3.

$$p_o \nabla \cdot \boldsymbol{u} + \frac{dp_o}{\gamma dt} = \frac{\gamma - 1}{\gamma}(\dot{q} + \nabla \cdot k \nabla T) \tag{5}$$

where $\gamma = c_p/c_v$. Integrating Equation 5 over the entire domain Ω yields a consistency condition for the background pressure $p_o(t)$,

$$p_o \int_{\partial\Omega} \boldsymbol{u} \cdot d\boldsymbol{S} + \frac{V dp_o}{\gamma dt} = \frac{\gamma - 1}{\gamma}\left(\int_\Omega \dot{q} dV + \int_{\partial\Omega} k \nabla T \cdot d\boldsymbol{S}\right) \tag{6}$$

where V is the volume of the enclosure. The background pressure can be expressed in terms of a background temperature $T_o(t)$ and density $\rho_o(t)$:

$$p_o = R \rho_o T_o \tag{7}$$

These spatially averaged quantities play the same role that ambient conditions do in the Boussinesq approximation. Perturbations to each are represented by the relations

$$T = T_o(t)(1 + \tilde{T}) \tag{8a}$$

$$\rho = \rho_o(t)(1 + \tilde{\rho}) . \tag{8b}$$

The perturbation values are thus simply related:

$$(1 + \tilde{T})(1 + \tilde{\rho}) = 1 . \tag{9}$$

Defining T_o and ρ_o through the adiabatic process yields

$$\frac{\rho_o}{\rho_\infty} = \left(\frac{p_o}{p_\infty}\right)^{\frac{1}{\gamma}}, \tag{10a}$$

$$\frac{T_o}{T_\infty} = \left(\frac{p_o}{p_\infty}\right)^{\frac{\gamma - 1}{\gamma}} . \tag{10b}$$

Substituting Equation 8b and the derivative with respect to time of Equations 8a and 10b into Equation 3, and simplifying, allows the energy equation to be expressed in terms of the perturbation temperature $\tilde{T}$ and the divergence:

$$\frac{\partial \tilde{T}}{\partial t} + \boldsymbol{u} \cdot \nabla T = (1 + \tilde{T})\left[\nabla \cdot \boldsymbol{u} + \frac{1}{\gamma p_o}\frac{dp_o}{dt}\right] \tag{11}$$

The background pressure is found from Equation 6.

In the momentum equation, the pressure is composed of three components, the background, the hydrostatic, and a perturbation to the hydrostatic,

$$p(\boldsymbol{r}, t) = p_o(t) - \rho_o(t) g z + \tilde{p}(\boldsymbol{r}, t) \tag{12}$$

where z is the vertical spatial component. After subtracting the hydrostatic pressure gradient from Equation 2 and then dividing by the density, the equation becomes

$$\frac{\partial \boldsymbol{u}}{\partial t} + \frac{1}{2}\nabla|\boldsymbol{u}|^2 - \boldsymbol{u} \times \omega + \frac{1}{\rho}\nabla\tilde{p} - \frac{\rho - \rho_o}{\rho}\boldsymbol{g} = \frac{1}{\rho}(\nabla \cdot \boldsymbol{\sigma}) . \tag{13}$$

To simplify this equation further, the density in the pressure term is assumed ambient and then the term $|\boldsymbol{u}|^2/2$ is combined with the perturbation pressure $\tilde{p}/\rho_o$ and written as a total pressure, H. Taking the divergence of Equation 13 yields a Poisson equation for the total pressure:

$$\nabla^2 H = \nabla \cdot \boldsymbol{F} - \nabla \cdot \boldsymbol{u} \tag{14}$$

where $\boldsymbol{F}$ represents the convective and diffusive terms of Equation 13.

The treatment of subgrid scale mixing follows very closely the analysis of Smagorinsky (1963).

The stress tensor σ in Equation 13 is replaced by the Reynolds stress tensor τ, whose components are written in the form

$$\tau_{ij} = 2\rho(C_s\Delta)^2|S_{ij}|S_{ij}$$

where

$$S_{ij} = \frac{1}{2}\left(\frac{\partial u_i}{\partial x_j} + \frac{\partial u_j}{\partial x_i}\right), \Delta = (\delta x \delta y \delta z)^{\frac{1}{3}}, |S_{ij}| = \sqrt{2S_{ij}}Sij,$$

and C_s is the Smagorinsky constant.

There have been numerous refinements of the original Smagorinsky model (Deardorff 1972; Germano et al. 1991; Lilly 1992), but it has been difficult to assess the improvements offered by these newer schemes for the fire scenarios to which the model has been applied. There are two reasons for this. First, the structure of the fire plume is so dominated by the large-scale, resolvable eddies that even a constant eddy viscosity gives results almost identical with those obtained here (Baum et al. 1996). Second, the lack of precision in most large-scale fire data makes it difficult to sort out the subtleties associated with these models. For the time being, the Smagorinsky model with the given C_s produces satisfactory results for most large-scale applications where boundary layers are not important.

In summary, the equations that are solved numerically are the energy equation (11), the momentum equation (13), and the Poisson equation for the total pressure (14). This linear Ielliptic equation is solved with the use of an FFT-based direct solver (GMS 1990). The background pressure, temperature, and density are found from Equations 6, 7, and 10. Each of the conservation equations emphasizes the importance of the divergence and vorticity fields, as well as the close relationship between the thermally expandable fluid equations (Rehm and Baum 1978) and the Boussinesq equations for which the authors have developed highly efficient solution procedures (McGrattan et al. 1994; Baum et al. 1994). The equations are discretized with second-order central differences. These are applied directly to the equations presented here with minor modifications and no loss in performance. The only changes from earlier methodology are a return to a uniform rectangular grid with blocks of cells masked to simulate internal boundaries and the use of a second-order Runge-Kutta scheme to advance the velocity and temperature fields in time. The speed and accuracy of this technique enable calculations on current generation workstations that involve more than a million computational cells, yielding the spatial range of two orders of magnitude for a three-dimensional calculation.

Flow in a Three-Dimensional Ventilated Room

The CFD program NIST-LES3D was applied to predict the flow in an isothermal, three-dimensional room (Figure 1). Both measurements (Restivo 1979) and CFD simulations (Davidson and Nielsen 1996) for this problem have been reported by others. Two levels of grid refinement were used

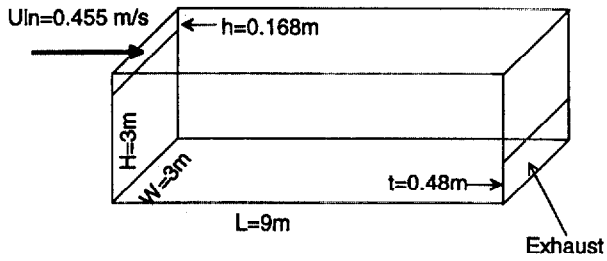

Figure 1 Three-dimensional ventilated room.

including 96 × 32 × 32 and 96 × 64 × 64. The Smagorinsky constant (C_s) used was varied between 0.1 and 0.23. The inlet velocity was 0.455 m/s with a uniform profile and no turbulence. Other boundary conditions included a pressure perturbation of 0 at the exhaust. Inlet conditions included no air motion and background P, T, and ρ throughout the room. Since the problem simulated is isothermal, $\nabla \cdot u = 0$, simulations were run for 600 seconds. Most calculations were performed on a computer with 192 Mb of RAM and took about 20 µs per time step per cell.

Results

Figure 2 shows calculated velocity vectors along the centerline plane of the ventilated room. These results are for a simulation grid of 96 × 64 × 64 and a Smagorinsky constant of 0.14 and show the main features of the flow including the jet from the inlet, the flow out the exhaust, and a large recirculation pattern through the main part of the room.

The velocity vectors shown in Figure 2 are for the instantaneous solution at a time of 600 seconds and cannot readily be compared to experimental results or evaluated further without time averaging. However, it is not obvious what time period should be used for the time averaging. Figures 3, 4, and 5 present normalized x velocities along a vertical line at $x/H = 1$ and $z/H = 0.5$ averaged over a variety of time periods. For this simulation, C_s was 0.14 and the grid was 96 × 32 × 32. Figure 3 shows results for averaging periods of 1 second (from 599 to 600 seconds), 10 seconds (from 590 to 600 seconds), and 100 seconds (from 500 to 600 seconds). A significant amount of noise due to turbulence exists for the 1-second and 10-second average periods. The pattern is considerably smoother for the 100-second average period. However, Figure 4 shows that a 100-second average is not sufficient to characterize the flow, as 100-second averages at successive times yield considerably different results. The Figure 4 results also show that the initial 100-second period is clearly affected by the initial conditions.

Figure 5 presents results averaged over successive 500-second periods with the initial 100 seconds discarded based on Figure 4. There is almost no visible difference between the successive periods, so little is gained in continuing the simulation beyond 600 seconds. Based on these comparisons, the remaining simulations were run for 600 seconds and results are presented as average velocities over the last 500 seconds.

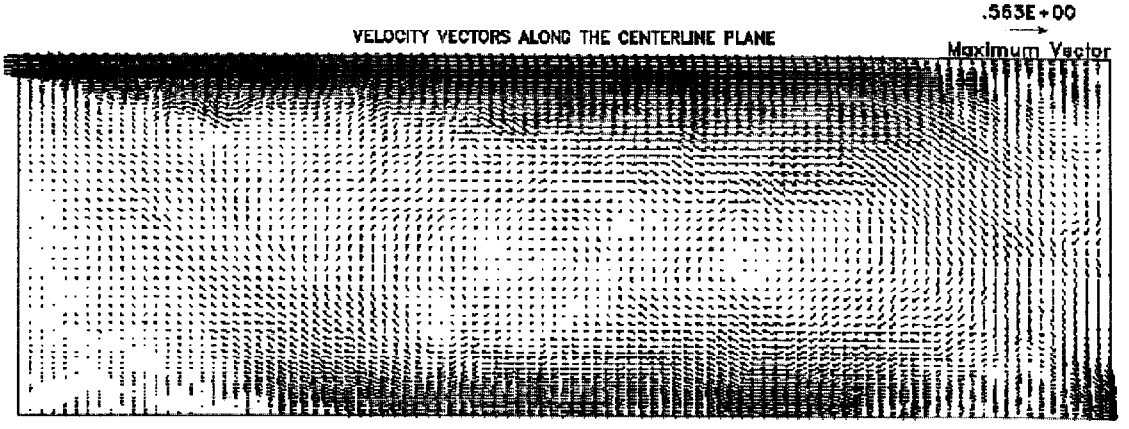

Figure 2 *Velocity vectors along the centerline plane.*

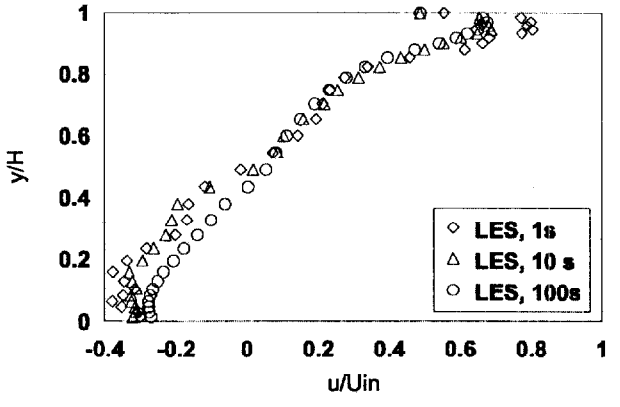

Figure 3 *Comparison of averaging periods.*

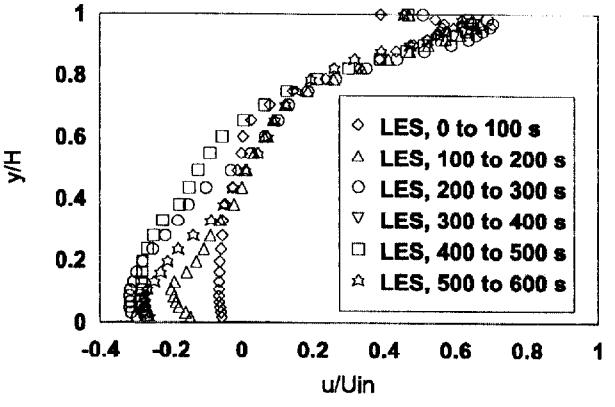

Figure 4 *Comparison of 100 s periods.*

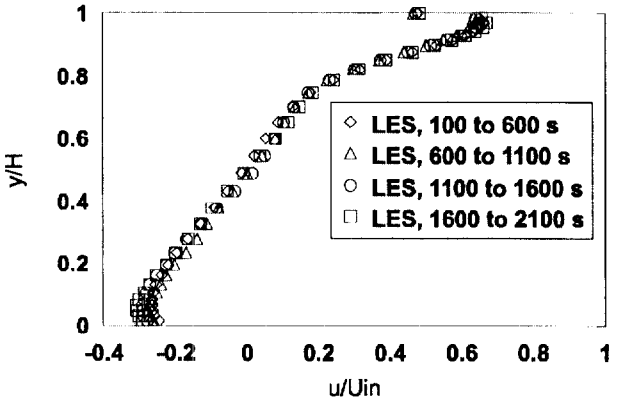

Figure 5 *Comparison of 500 s periods.*

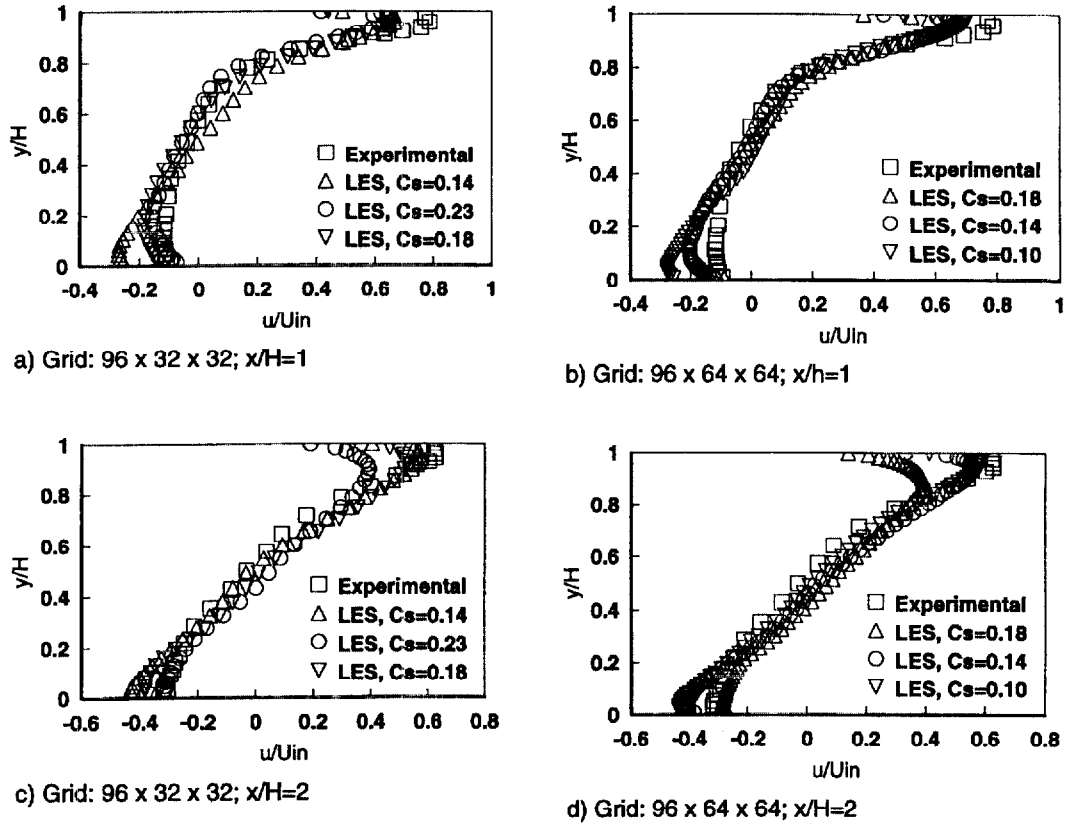

Figure 6 *Comparison of LES results to experimental (varied grid and Smagorinsky constant).*

Figure 6 compares normalized X velocities for various simulation cases to experimental measurements. Figures 6a and 6b show results along the same vertical line as Figures 3, 4, and 5 for grids of $96 \times 32 \times 32$ and $96 \times 64 \times 64$, respectively, and C_s varied in a range of 0.10 to 0.23. Figures 6c and 6d present similar results for the same simulations as Figures 6a and 6b but further downstream from the ventilation supply at $x/H = 2$. All of these simulations capture the airflow pattern in the main portion of the room, with the greatest discrepancy existing near the floor and ceiling.

A quantitative comparison of the simulation and experimental results is presented in Table 1, which shows the average differences between the calculated and measured X velocities as a percent of the inlet velocity at 11 vertical locations of the results in Figure 6 (at the measurement location nearest the floor and ceiling and at nine equally spaced points along the line). The differences are expressed relative to the inlet velocity to avoid the problem of calculating percent differences for very small velocities. The choice of Smagorinsky constant has an impact on the results that appear to inter-

TABLE 1
Comparison of LES and Experimental Results

Simulation Case		Average Difference ($x/H = 1$)	Average Difference ($x/H = 2$)	Average Difference (Both)
Grid	C_s			
96×32×32	0.14	7.5	5.7	6.6
96×32×32	0.18	4.5	7.2	5.8
96×32×32	0.23	4.2	8.7	6.4
96×64×64	0.1	6.6	4.8	5.7
96×64×64	0.14	5.4	5.8	5.6
96×64×64	0.18	7.1	11.1	9.1

act with the grid refinement. For the coarser grid, the closest comparison to measured values is obtained with $C_s = 0.18$ (see Figures 6a and 6c), while $C_s = 0.14$ appears to give the best comparison for the finer grid (see Figures 6b and 6d).

As stated earlier, Davidson and Nielsen (1996) identified strong dependence (both flow and grid dependence) of simulation results on the Smagorinsky constant as a major drawback for this model. Some evidence for both types of dependence are apparent in the Figure 6 and Table 1 results. Bennetsen et al. (1996) also cited problems with grid resolution for the simulations with the Smagorinsky model. Due to dissatisfaction with the Smagorinsky results, Davidson and Nielsen (1996) abandoned the Smagorinsky model and continued simulations with the more complex dynamic subgrid-scale model.

Figures 7a and 7b present a comparison with the "best" Smagorinsky LES simulation based on the differences in Table 1 results to both Davidson and Nielsen's dynamic LES simulation result and the measured values. The Smagorinsky LES results are for a grid of 96 × 64 × 64 and $C_s = 0.14$. The Davidson and Nielsen dynamic LES simulation used a grid of 102 × 52 × 52. Figures 7a and 7b present results along the same vertical lines as Figure 6, while Figure 7c presents normalized X velocities along a line near the ceiling running the length of the room at the midpoint and Figure 7d presents normalized X velocities along a similar line near the floor.

The simulation using the dynamic subgrid-scale model has a distinct advantage over the one with the Smagorinsky near the floor and ceiling (see Figures 7c and 7d), but there is no clear difference in the bulk portion of the room (see Figures 7a and 7b). However, the difference near the floor and ceiling may not be due to any advantage of the dynamic model, as Davidson and Nielsen (1996) also used an additional empirical model for the near wall region and such a model was not used for the Smagorinsky simulations. Also, a detailed comparison of results near the floor and ceiling is difficult, as the exact location of the measurements is not known and a small difference in location in this region can have a large impact on the results.

Since both models result in good agreement with the experimental results in the main portion of the room, the main advantage of the dynamic model is relief from selecting an appropriate value for C_s. Since the present work emphasizes obtaining a relatively fast solution using efficient solving techniques, this advantage may not be worth pursuing in the present context. However, if the flow near the wall is of particular interest, the use of a near wall model may be applied.

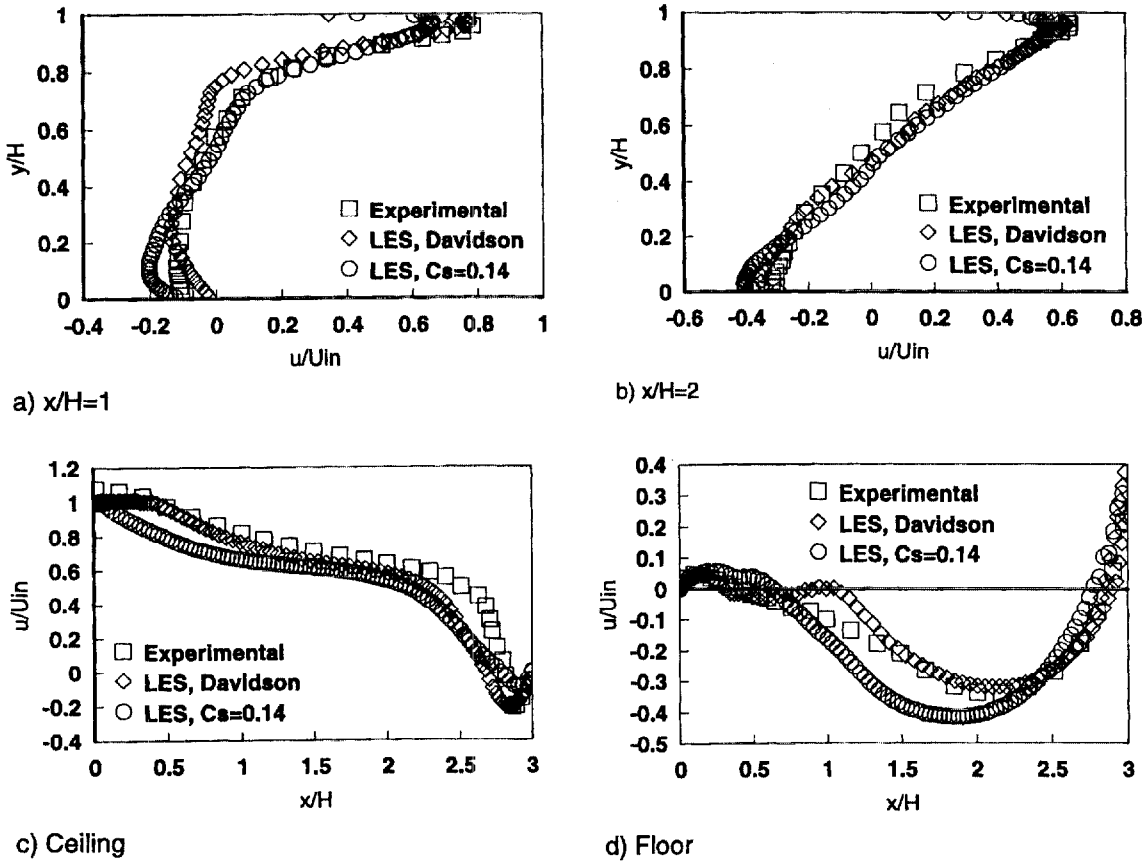

Figure 7 Comparison of LES results to Davidson simulation and experimental.

CONCLUSIONS

The application of a large eddy simulation CFD model to study building ventilation has been described. The model was originally developed to study fire situations and emphasizes high spatial resolution and efficient solution techniques. A literature review indicated that LES has the potential to simulate turbulent flow in room airflow problems better than the typical k-ε model and that several researchers are working with LES models.

The LES model with the Smagorinsky subgrid-scale model was applied to model ventilation airflow in a three-dimensional room. Airflow results were in excellent agreement with both measured values and LES simulations, with more complicated dynamic SGS model (reported by Davidson and Nielsen [1996]) in the main portion of the room. Agreement was not as good near the floor and ceiling; however, no empirical near-wall model was used. Also, some evidence of interaction between Smagorinsky constant and grid resolution was found.

REFERENCES

Anderson, D.A., J.C. Tannehill, and R.H. Pletcher. 1984. *Computational fluid mechanics and heat transfer.* New York: Hemisphere Publishing Company.

Baum, H.R., O.A. Ezekoye, K.B. McGrattan, and R.G. Rehm. 1994. Mathematical modeling and computer simulation of fire phenomena. *Theoretical and Computational Fluid Dynamics* 6:125-139.

Baum, H.R., K.B. McGrattan, and R.G. Rehm. 1996. Three-dimensional simulations of fire plume dynamics. *J. of the Heat Transfer Society of Japan* 35:45-52.

Bennetsen, J., J.N. Sorensen, H.T. Sogaard, and P.L. Christiansen. 1996. Numerical simulation of turbulent airflow in a livestock building. *Roomvent '96,* Vol. 2.

Buchmann, P., J. Riberon, J.R. Millet, and G. Lauriat. 1994. Numerical predictions of airflow patterns in large enclosures with supplied air jet system." *Roomvent '94.*

Chen, Q., and N.-T. Chao. 1996. Prediction of buoyant plume and displacement ventilation with different turbulence models. *Indoor Air,* Vol. 1.

GMS. 1990. *Crayfishpak user's guide,* Version 1.1. Boulder, Colo.: Green Mountain Software.

Davidson, L., and P.V. Nielsen. 1996. Large eddy simulation of the flow in a three-dimensional ventilated room. *Roomvent '96,* Vol. 2.

Deardorff, J.W. 1970. A numerical study of three-dimensional turbulent channel flow at large Reynolds numbers. *J. Fluid Mech.* 41.

Deardorff, J.W. 1972. Numerical investigation of neutral and unstable planetary boundary layers. *J. Atm. Sciences* 29:91-115.

Emmerich, S.J. 1997. *Use of computational fluid dynamics to analyze indoor air quality issues.* NISTIR 5997, National Institute of Standards and Technology.

Germano, M., U. Piomelli, P. Moin, and W.H. Cabot. 1991. A dynamic subgrid-scale eddy viscosity model. *Physics of Fluids A* 3:1760-1765.

Kurabuchi, T., J.B. Fang, and R.A. Grot. 1990. *A numerical method for calculating indoor airflows using a turbulence model.* NISTIR 89-4211, National Institute of Standards and Technology.

Kurabuchi, T., and T. Kusuda. 1987. Numerical prediction for indoor air movement. *ASHRAE Journal,* December.

Lilly, D.K. 1992. A proposed modification of the Germano subgrid-scale closure method. *Physics of Fluids A* 4:633-635.

McGrattan, K., R.G. Rehm, and H.R. Baum. 1994. Fire-driven flows in enclosures. *Journal of Computational Physics* 110:285-291.

Moser, A. 1991. The message of Annex 20: Air flow patterns within buildings. 12th AIVC Conference.

Murakami, S., S. Kato, and R. Ooka. 1994. Comparison of numerical predictions of horizontal nonisothermal jet in a room with three turbulence models—k-ε ESM, ASM, and DSM. *ASHRAE Transactions* 100(2):697-704. Atlanta: American Society of Heating, Refrigerating and Air-Conditioning Engineers, Inc.

Murakami, S., A. Mochida, R. Ooka, S. Kato, and S. Iizuka. 1996. Numerical prediction of flow around a building with various turbulence models: Comparison of k-ε EVM, ASM, DSM, and LES with wind tunnel tests. *ASHRAE Transactions* 102(1):741-753. Atlanta: American Society of Heating, Refrigerating and Air-Conditioning Engineers, Inc.

Rehm, R.G., and H.R. Baum. 1978. The equations of motion for thermally driven, buoyant flows. *Journal of Research of the NBS* 83:285-291.

Restivo, A. 1979. *Turbulent flow in ventilated rooms.* University of London, Mechanical Engineering Dept.

Sakamoto, Y., and Y. Matsuo. 1980. Numerical predictions of three-dimensional flow in a ventilated room using turbulence models. *Appl. Math. Modeling* 4 (Feb.).

Smagorinsky, J., S. Manabe, and J.L. Holloway. 1965. Numerical results from nine-level general circulation model of the atmosphere. *Mon. Weath. Rev.* 93.

Smagorinsky, J. 1963. General circulation experiments with the primitive equations. *Mon. Weath. Rev.* 91.

Stathopoulos, T., and Y.S. Zhou. 1995. Evaluation of wind pressures on flat roofs. *Building and Environment* 30.

Takemasa, Y., T. Kurabuchi, and M. Kamata. 1992. Numerical simulation of indoor temperature and wall heat flow distribution of a heated and cooled room. *Room Air Convection and Ventilation Effectiveness.* Atlanta: American Society of Heating, Refrigerating and Air-Conditioning Engineers, Inc.

Tennekes, H., and J.L. Lumley. 1972. *A first course in turbulence.* MIT Press.

Walton, G.N. 1994. CONTAM93—User's manual. NISTIR 5385, National Institute of Standards and Technology.

Xu, J., H. Liang, and T.H. Kuehn. 1994. Comparison of numerical predictions and experimental measurements of ventilation in a room. *Roomvent '94,* Vol. 2.

Zhou, Y., and T. Stathopoulos. 1996. Application of two-layer methods for the evaluation of wind effects on a cubic building. *ASHRAE Transactions* 102(1):754-764. Atlanta: American Society of Heating, Refrigerating and Air-Conditioning Engineers, Inc.